Ion recombination correction factors and detector comparison in a very-high dose rate proton scanning beam

A.M.M. Leite, M. Cavallone, M.G. Ronga, Francois Trompier, Yoann Ristic, L. de Marzi, A. Patriarca

Physica Medica 106 (2023) 102518

Contents lists available at ScienceDirect

Physica Medica

journal homepage: www.elsevier.com/locate/ejmp

Ion recombination correction factors and detector comparison in a very-high dose rate proton scanning beam

A.M.M. Leite [a,b,*], M. Cavallone [b], M.G. Ronga [b], F. Trompier [c], Y. Ristic [c], A. Patriarca [b], L. De Marzi [b,d,*]

[a] Institut Curie, PSL Research University, Université Paris-Saclay, CNRS UMR 3347, INSERM U1021, 91898 Orsay, France
[b] Institut Curie, PSL Research University, Radiation Oncology Department, Proton Therapy Center, Centre Universitaire, 91898 Orsay, France
[c] Institut de Radioprotection et de Sûreté Nucléaire, Service de Dosimétrie, Laboratoire de Dosimétrie des Rayonnements Ionisants, 92262 Fontenay-aux-Roses Cedex, France
[d] Institut Curie, PSL Research University, Université Paris-Saclay, INSERM LITO, 91898 Orsay, France

ARTICLE INFO

Keywords:
Proton therapy
Experimental dosimetry
Ion chamber
Very-high dose rate
FLASH
Ion recombination

ABSTRACT

Purpose: Accurate dosimetry is paramount to study the FLASH biological effect since dose and dose rate are critical dosimetric parameters governing its underlying mechanisms. With the goal of assessing the suitability of standard clinical dosimeters in a very-high dose rate (VHDR) experimental setup, we evaluated the ion collection efficiency of several commercially available air-vented ionization chambers (IC) in conventional and VHDR proton irradiation conditions.

Methods: A cyclotron at the Orsay Proton Therapy Center was used to deliver VHDR pencil beam scanning irradiation. Ion recombination correction factors (k_s) were determined for several detectors (Advanced Markus, PPC05, Nano Razor, CC01) at the entrance of the plateau and at the Bragg peak, using the Niatel model, the Two-voltage method and Boag's analytical formula for continuous beams.

Results: Mean dose rates ranged from 4 Gy/s to 385 Gy/s, and instantaneous dose rates up to 1000 Gy/s were obtained with the experimental set-up. Recombination correction factors below 2 % were obtained for all chambers, except for the Nano Razor, at VHDRs with variations among detectors, while k_s values were significantly smaller (0.8 %) for conventional dose rates.

Conclusions: While the collection efficiency of the probed ICs in scanned VHDR proton therapy is comparable to those in the conventional regime with recombination coefficiens smaller than 1 % for mean dose rates up to 177 Gy/s, the reduction in collection efficiency for higher dose rates cannot be ignored when measuring the absorbed dose in pre-clinical proton scanned FLASH experiments and clinical trials.

Introduction

Radiotherapy is a curative treatment for a large variety of cancers and is one of the key components of effective cancer treatment, comprising 50 % to 60 % of cancer treatments. It operates on a thin line between maximizing the eradication of tumour cells while minimizing the damage to nearby healthy tissues. Already observed in 1959 by Dewey and Boag [1], the effect of large doses delivered in a short time was recently brought to the spotlight by Favaudon et al. [2] who used an electron accelerator to produce mean dose rate electron beams greater than 40 Gy/s, and observed that FLASH-irradiated mice did not exhibit pneumonitis and lung fibrosis, unlike conventional dose rate ($\leq$0.03 Gy/s) irradiated mice, while retaining tumour control – FLASH effect. FLASH radiation therapy (FLASH-RT) may open the door to an increase of the therapeutic index, allowing for dose escalation especially relevant to radio-resistant tumours, such as glioblastoma, and to potentially circumvent the motion-induced uncertainties of the delivered radiation, given that the time scale of the irradiation itself is much shorter than any patient's movement. In FLASH-RT the therapeutic dose is delivered within a few milliseconds (Very-High dose rate or VHDR) or microseconds (Ultra-High dose rate or UHDR), while in conventional radiation therapy (CONV-RT) irradiations take a few minutes (in what follows, we

* Corresponding authors at: Institut Curie, PSL Research University, Radiation Oncology Department, Proton Therapy Center, Centre Universitaire, 91898 Orsay, France.
E-mail addresses: amelia.leite@ijclab.in2p3.fr (A.M.M. Leite), ludovic.demarzi@curie.fr (L. De Marzi).

https://doi.org/10.1016/j.ejmp.2022.102518
Received 30 March 2022; Received in revised form 9 December 2022; Accepted 27 December 2022
Available online 11 January 2023

will use this convention for the definition of dose rates). Since the first seminal work of Favaudon et al. the FLASH effect has been confirmed across multiple tissue types [2–9], animal models and for various particle types including photons [10], electrons [11] and protons [5,12]. Recently, the first patient was successfully treated with electron FLASH-RT for subcutaneous T-cell lymphoma [13] with also positive outcome for normal skin tissues. Currently, a clinical study [14] is underway in the USA to investigate the feasibility of proton FLASH-RT for the palliative treatment of painful bone metastases.

Clinical proton therapy beamlines can be modified to be capable of (pre-) clinical studies in the FLASH regime, with many proton therapy centers already reporting the successful delivery of FLASH proton beams either with cyclotrons [5,12,15,16], or synchrocyclotrons [17,18]. For that reason, it is paramount to characterize the already available dosimetric tools in the conditions of proton FLASH dose rates and envision possible technological upgrades [19,20]. Ionization chambers are routinely used in radiotherapy and are the reference tools for the measurement of the absorbed dose in clinical dosimetry [21,22], although at the present moment no recommendations or dosimetric protocols exist for FLASH-RT. Ionization chambers exhibit a reduction of the charge collection efficiency due to the recombination of ions along the original ionization track before reaching the collecting electrodes – initial recombination [23]. This effect is more predominant in high linear energy transfer beams or regions at the distal end of the Bragg peak, in which the ionization density is higher. In addition, ions belonging to different ionization tracks can combine with each other, thereby reducing the charge collected by the ionization chamber - volume recombination [24]. This mechanism is highly dependent on the ionization current and, consequently, on the dose rate, and in FLASH dose rates it becomes the dominant effect that leads to the reduction of the collected charge. The recombination coefficient, k_s - inverse of the charge collection efficiency, needs to be determined for each chamber as it is voltage and geometry-dependent.

Substantial work has already been carried out on pulsed electron FLASH dosimetry. However, current theoretical models [25,26], largely based on Boag's work [27], present a number of limitations in high dose-per-pulse (DPP) beams [28]. The Two-voltage method (TVM) recommended by the International Atomic Energy Agency (IAEA) TRS-398 [21] dosimetry protocol, and also based on Boag's model [29], does not take into account the fraction of free electrons that are collected by the electrodes without inducing any ionization, which can result in the underestimation of the ion collection efficiency in high DPP beams. In narrow chambers, operated at high voltages and in high DPP beams, the space charge results in a distortion of the electric field leading to a reduction of the field strength inside the ionization chamber, and consequently to a greater ionic recombination. Petersson et al. [30] proposed an empirical model to correct the ion recombination in the Advanced Markus chamber in high DPP electron beams (10^{-4} Gy–10 Gy) for recommended polarization voltages. The ion collection efficiency was shown to decrease with increasing DPP, while remaining unaltered with the dose rate, and k_s values were higher than 3. Gotz et al. [31] developed a numerical model of the transport of charges in a plane-parallel ionization chamber that includes the effect of the charges and their inhomogeneous distribution on the chamber's electric field. Furthermore, the model showed a better agreement with measurements done with a PTW Advanced Markus chamber at higher collection bias, than Boag's theory and was in agreement with the empirical model of Petersson et al. [30].

The dose rate in conventional proton pencil beam scanning (PBS), with instantaneous dose rates of a few Gy/s, is much higher than in scattered beams, which can therefore significantly modify the charge collection and recombination factors expected in ionization chambers. The ion recombination effect has already been evaluated in scanned beams by several groups employing different methods. Liszka et al. [32] evaluated the ion recombination of an air-vented ionization chamber in conventional continuous PBS beams and observed a dependency on the beam energy and dose rate, the two being correlated, concluding that volume recombination should not be disregarded and that recombination coefficients ought to be determined for each employed chamber and beam quality. Rossome et al. [33] have proposed an alternative method to the TVM for protons and light-ion beams, using three current measurements at three different polarizing voltages (V), to determine the saturation current, provided that the linearity of k_s with $1/V$ (pulsed beams) and $1/V^2$ (continuous beams) can be established. This method, appropriately called the three-voltage linear method, was shown to be more accurate than the TVM since the use of three voltages ensures the verification of the previously mentioned linearity. Yin et al. [34] compared the TVM and the three-voltage method to theoretical values of ion recombination coefficients in passive scattering proton FLASH conditions. A good agreement was observed among the three methods for parallel-plate chambers for mean dose rates of up to 127.58 Gy/s; however, they concluded that cylindrical chambers, such as the IBA CC13 chamber or larger chambers, should not be employed in proton FLASH dosimetry as ion recombination correction values were larger than 50 % for dose rates $\geq$ 63.71 Gy/s. Cunningham et al. [12] reported that in a FLASH PBS beam with doses rate up to 115 Gy/s, the recombination effects in the Advanced Markus chamber are smaller than 1.0 %.

In our previous work [15], we have developed an experimental set-up capable of performing FLASH-PT irradiations, based on scattered beams. We have characterized this system using dosimetric methods and compared several detectors, for mean dose rates up to 80 Gy/s. Motivated by the growing evidence and support for FLASH, we report in this work the characterisation of a new set-up dedicated to pre-clinical experiments and based on scanned beams, capable of VHDR irradiations with instantaneous dose rates of 1000 Gy/s. Scarce data or experimental set-ups exist at these dose rate conditions, or at least for this configuration of a clinical machine, so we propose an evaluation of the recombination factors for a set of detectors with different geometries, some of which commonly used in proton therapy, and the comparison of experimental results with theoretical models.

2. Materials and methods

In this work we studied the charge collection efficiency of several air-vented ionization chambers with different geometries (at different depths in water) in VHDR beams, and compared them to the conventional irradiation regime. Herein, we define mean dose rate as the total dose over the total deliver time; instantaneous dose rate as the dose rate of a single pencil beam; and since each pencil beam contributes with a different dose to the total dose measured in an ionization chamber, we define the mean effective dose rate, $\dot{D}_{eff}$, using the following expression [32]:

$$\dot{D}_{eff} = \frac{\sum_{i=1}^{N} D_i \bullet \dot{D}_i}{\sum_{i=1}^{N} D_i} \quad (1)$$

where D_i is the dose of the i-th pencil beam with instantaneous dose rate $\dot{D}_i$.

The evaluated chambers were the PPC05, the CC01 and the Razor Nano-chamber CC003 (IBA Dosimetry, Schwarzenbruck, Germany), and two PTW Advanced Markus type 34,045 (PTW, Freiburg im Breisgau, Germany) with series number (SN) 870 and 879. Their characteristics are summarised in Table 1. We also estimated the response of the PTW microDiamond Type 60019, detector, which is indicated for small field dosimetry, and the IBA Razor Diode detector, with no external bias voltage applied, as their response to such dose rate levels has never been reported.

Recombination coefficients of ionization chambers can be evaluated using Niatel's model [35] that combines initial and volume recombination ($k_s = k_s^{ini}\, k_s^{vol}$), and has already been applied in scanned proton beams in conventional dose rates [32,33,36]:

Table 1
Properties of the ionization chambers and semiconductor detectors investigated in this work. Ionization chamber quantities were obtained from vendor websites (https://www.ptwdosimetry.com, https://www.iba-dosimetry.com) unless a literature reference is given.

	SN	Geometry	Sensitive volume (mm^3)	Sensitive volume radius (mm)	Electrode separation (mm)	Operating voltage (V)	Collection time (μs)	g (m)
Advanced Markus	870, 879	Plane-parallel	20	2.5	1	300	22	8E-6
PPC05	868	Plane-parallel	46	4.95	0.6	300	7 [41]	5E-7
Nano Razor CC003	15640	Spherical	3	1	0.5	300	5 [42]	5E-6
CC01	10308	Cylindrical	10	1	1	300	N/A	4E-5
microDiamond	122691	Disk	0.004	1.1	N/A	0	N/A	N/A
Razor Diode	10559	Disk	0.006	0.3	N/A	0	N/A	N/A

$$k_s(\mathrm{V}) = \frac{Q_{sat}}{Q(V)} = 1 + \frac{A}{V} + \frac{B}{V^2}Q_{sat} \tag{2}$$

where the term A/V corresponds to initial recombination and B/V^2 accounts for volume recombination effects. The charge saturation value,Q_{sat}, is then obtained by fitting the curves of the inverse of the collected charge, $1/Q$, versus the inverse of the square of the chambers' polarizing voltage, $1/V^2$, for continuous beams with the polynomial

$$\frac{1}{Q(V)} = \frac{1}{Q_{sat}} + \frac{\alpha}{V} + \frac{\beta}{V^2} \tag{3}$$

where $\alpha = A/Q_{sat}$ and$\beta = B$. In addition, the TVM can also be applied to estimate the volume recombination when initial recombination can be ignored, which for continuous beams follows the expression:

$$k_s = \frac{\left(\frac{V_1}{V_2}\right)^2 - 1}{\left(\frac{V_1}{V_2}\right)^2 - \frac{Q_1}{Q_2}} \tag{4}$$

where V_i is the polarizing voltage used to measure the charge Q_i. In this work, we used $V_1 = 300$ V and $V_2 = 100$ V. This method is based on Boag's model and is applicable in the linear regime of the inverse of the charge with the inverse of the applied voltage to the chamber for pulsed beams, and the inverse of the square of the applied voltage for continuous beams [29]. Both CONV and VHDR proton pencil beams can be considered continuous, as the bunch duration was much shorter than the considered chambers' collection time (few μs) and the RF frequency of the cyclotron was 106 MHz [37,38].

We applied a third method as described by Liszka et al. [32], and based on the work of Palmans et al. [39], to calculate the volume recombination collection efficiency using Boag's analytical formula:

$$k_s = 1 + \frac{m^2 g}{V^2} I_{V,eff} \tag{5}$$

where m^2 is a volume recombination parameter [40] ($3.97 \bullet 10^{14}$ $sm^{-1}C^{-1}V^2$), g is a parameter dependent on the geometry of the chamber, ν is the ionization chamber's volume and V the applied bias. The mean effective current,$I_{V,eff}$, was calculated considering the individual contribution of each beam spot to the total current measured by the chamber, as well as the spot's duration, similarly to eq. (1).

2.1. Experimental set-up

The Proton Therapy Center at Institut Curie houses one "universal" nozzle-equipped gantry supplied by a Proteus 235 isochronous cyclotron (IBA, Belgium) capable of delivering both pencil beam scanning and double scattering (DS) treatment modalities and also very-high dose rate irradiation. This model has already been used by several groups to perform FLASH irradiations using different experimental set-ups, for example with single scattered [15], double scattered [5,34] or scanned beams. In our VHDR set-up with scanned beams, the dose rate was maximized by using the maximum nominal cyclotron current of 500 nA and 226.899 MeV energy, as any energy degrader introduces substantial losses, besides the optimization of the beam transport. The pencil beam scanning, performed with two scanning magnets, was also optimised to reduce the dead time between each pencil beam position. With this specific set-up, also used for radiobiology experiments, an initially accelerated narrow monoenergetic proton pencil beam (in our case the spatial spread of the pencil beam is 4.0 ± 0.3 mm in air at isocenter) can be scanned over a 15×15 mm^2 square field (a uniform broad field is generated by the superposition of a finite number of equally-spaced proton pencil beams), thus satisfying a priori requirements of VHDR irradiation for healthy tissues (the constraint that we have adopted is that the irradiation duration has to be shorter than 100 ms and mean dose rates are greater than 100 Gy/s). The electrometer of the monitoring ionization chambers was adapted with a resistive divider to ensure its operation in VHDR mode, and the delivery system control files [43] (or log files) were used to characterize the time structure of the VHDR beams, necessary to estimate instantaneous and mean dose rates. The read-out of the monitoring ionization chambers was performed every 250 μs, which is shorter than the delivery time of each pencil beam (the minimum spot duration was set to 1 ms). In this configuration each pencil beam had a duration of approximately 7 ms with a total irradiation time of 99 ms for FLASH irradiations of 17.5 Gy. A description of the experimental set-up is shown in Fig. 1, in which one can see the distribution of the spots, as well as the way the dose varies spatially and over time during the irradiation. The physical properties of the irradiation fields used in this work are summarized in Table 2. In particular, we can see in this figure that the spatial dose rate distribution in a PBS plan depends on the arrangement and the distance between the pencil beams. When the dose rate dependence of the detector response is no longer negligible, and especially if the detector is small, it may then be necessary to take into account the effective dose rate at the measurement point in order to correctly evaluate the detector response.

Throughout this work, reference dosimetry was performed with the Advanced Markus chamber (SN 870) calibrated under reference conditions at the PTW-Freiburg calibration laboratory (Freiburg, Germany) in terms of absorbed dose-to-water. We applied the calibration coefficient of 1.4466 Gy/nC, the polarity correction factor of 1 [32], the beam quality correction factor of 1.004 [44], the ion recombination correction obtained as in section 2.1 and the temperature and pressure correction factor.

Ion collection efficiencies for CONV and VHDR irradiations were evaluated at the plateau region of the Bragg peak curve (2 cm depth in water), corresponding to a mean dose rate measured with the Advanced Markus chamber (SN 870) of 4.1 Gy/s (7.0 Gy/s mean effective dose rate) and 177 Gy/s (437 Gy/s mean effective dose rate), respectively, and at the Bragg Peak (29.4 cm depth in water), corresponding to 385 Gy/s in the VHDR mode (951 Gy/s mean effective dose rate). The IBA BluePhantom was used for precise positioning of the ionization chambers. Recombination coefficients were also evaluated for different instantaneous dose rates, corresponding to the contributions of the

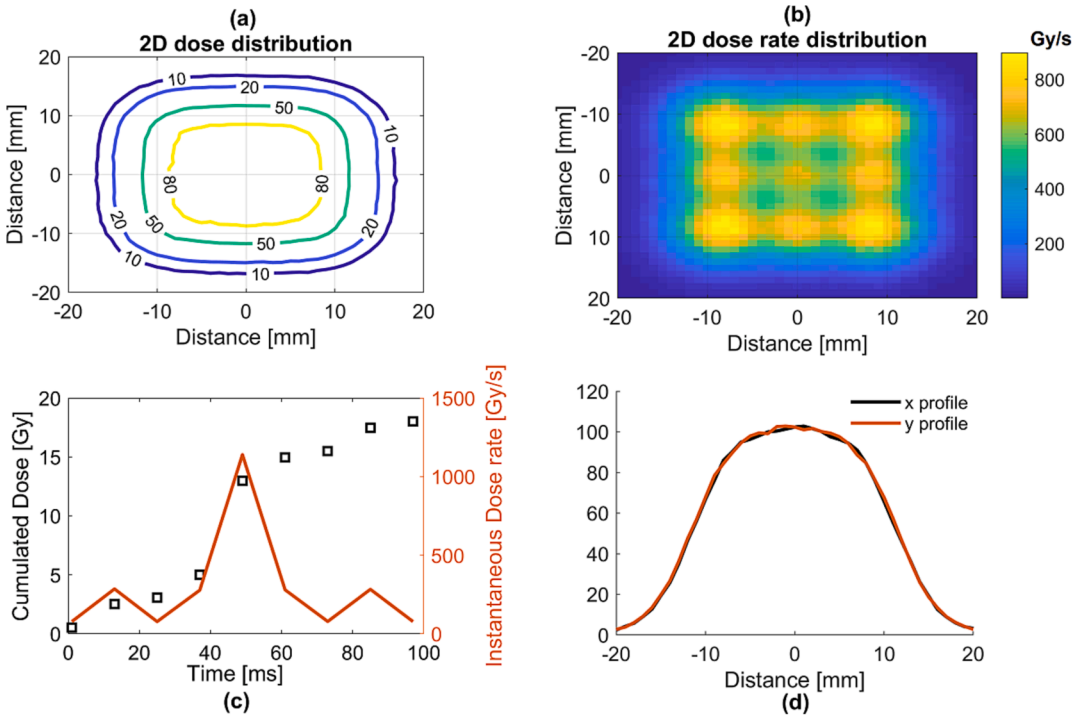

Fig. 1. Description of the experimental setup (plateau region of the Bragg peak curve, 2 cm depth in water): (a) 2D dose distribution of all spots, (b) corresponding dose rate distribution according to equation (1). (c) Cumulated and instantaneous dose rate as a function of time at the center of the field and (d) central dose profiles measured with the 2D scintillator detector Lynx (IBA Dosimetry).

Table 2
Properties of the irradiation field. The given current corresponds to the current at the exit of the cyclotron.

	Depth in water (cm)	Current (nA)	Dose (Gy)	Mean dose rate (Gy/s)	Mean effective dose rate (Gy/s)	Total irradiation time (ms)	Pencil beam irradiation time (ms)
CONV	2 ± 0.5 %	110	4.37 ± 2 %	4.1 ± 2 %	7.0 ± 2 %	1066 ± 0.02 %	125 ± 0.2 %
VHDR plateau	2 ± 0.5 %	500	17.5 ± 2 %	176.8 ± 0.2 %	437 ± 0.2 %	99 ± 0.2 %	7.25 ± 3.4 %
VHDR Bragg peak	29.4 ± 0.03 %	500	38.1 ± 2 %	384.8 ± 0.2 %	951 ± 0.2 %	99 ± 0.2 %	7.25 ± 3.4 %

different pencil beams to the total dose of the irradiated field measured with the Advanced Markus chamber (SN 870): this was achieved by measuring the dose delivered by each of the pencil beams composing the square field, irradiating them one by one, sequentially. This procedure was repeated for four different polarizing voltages and Niatel's model was applied to obtain the coefficients. The IBA Dose1 electrometer (IBA-Dosimetry, Schwarzenbruck, Germany) was used to read the charge collected by the ionization chambers and to apply the polarizing voltage. We measured the integrated charge for different polarizing voltages: 100 V, 150 V, 200 V, 300 V, 400 V and recorded five measurements for each voltage.

3. Results

Three methods were applied to calculate the ion recombination coefficients of five ionization chambers with different dimensions and geometries: Niatel's model, the TVM and Boag's analytical formula. Fig. 2a shows normalized plots of $1/Q$ as a function of $1/V^2$ obtained in CONV irradiation conditions measured at the plateau of the Bragg peak curve, while Figs. 3 and 4 show the equivalent plots in VHDR conditions, both measured at the plateau and at the Bragg peak. The error bars correspond to 1 standard deviation of the mean. The plots were fitted with a linear fit (Fig. 3) and with a polynomial fit corresponding to eq. (3) (Fig. 4). In both CONV and VHDR conditions the data points at the polarizing voltage of 400 V were not considered in the fit of both Advanced Markus chambers, since it appears to be a distortion due to the effect of charge multiplication, confirmed by plotting $1/Q$ versus $1/V$.

The fitting parameters of the polynomial fits (obtained from non-normalized plots) are presented in Table 3, along with 95 % confidence intervals evaluated with the Student's t-distribution. Table 4 summarizes the ion recombination coefficients determined for CONV (4.1 Gy/s) and VHDR irradiations, the latter includes coefficients evaluated at the entrance plateau, corresponding to the mean dose rate of 177 Gy/s, and at the Bragg peak, corresponding to the mean dose rate of 385 Gy/s. Fig. 2b shows k_s, calculated with eq. (2), as a function of the inverse of the polarizing voltage for CONV conditions, the equivalent is presented in Fig. 5 for VHDR conditions.

In Fig. 6a, one can observe that the IBA PPC05 chamber exhibits the highest collection efficiency among the tested chambers, which is expected since the electrode separation is the smallest. Even though the Advanced Markus, the Nano Razor and the CC01 chambers have a smaller sensitive volume than the PPC05, their larger electrode spacing results in higher ion recombination. A comparison between the methods used to evaluate k_s for the different chambers is shown in Fig. 6b and Table 4. The assumption of linearity of our measurements can be established, as one can observe in Fig. 3a that for FLASH dose rates all chambers are in the linear regime ($R^2 > 0.9$), except for the PPC05 chamber; therefore, the TVM and Boag's methods should be applicable. The observed differences of k_s values between the different models are within the experimental uncertainties, with the exception of the Nano

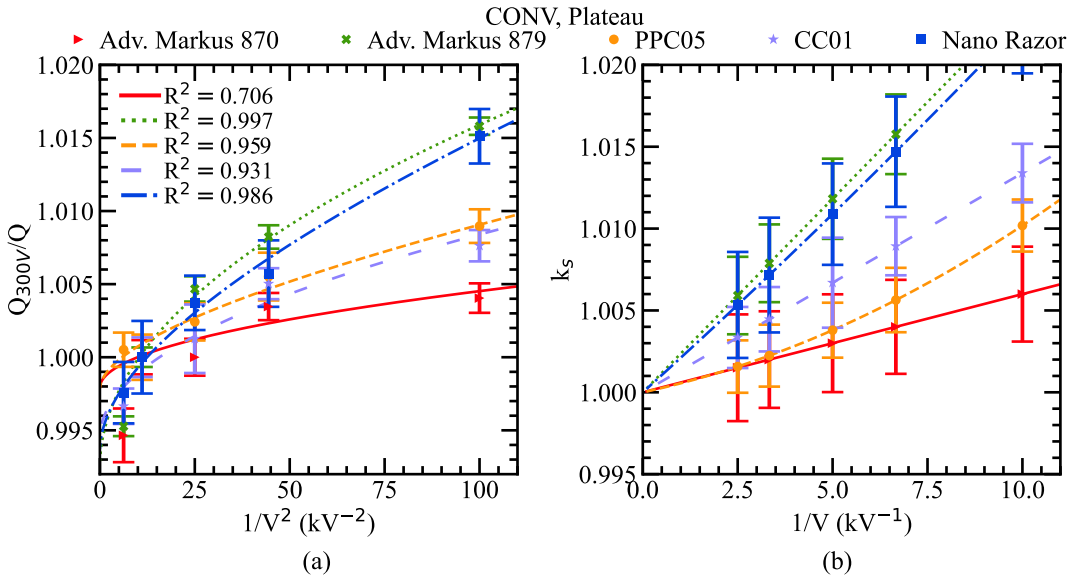

Fig. 2. (a) The inverse of the collected charge, $1/Q$, normalized to the collected charge with the ionization chamber biased to 300 V, Q_{300V}, as a function of the inverse of the chamber's polarizing voltage, $1/V^2$, for the Advanced Markus SN 870 and SN 879, the PPC05, the CC01 and the Nano Razor CC003 chamber. The measurements were performed in CONV conditions at the plateau of the Bragg peak. The lines correspond to polynomial fits as in eq. (3), respective R^2 are shown. (b) k_s values as a function of the inverse of the ionization chambers' bias, $1/V$, obtained with the polynomial fit, eq. (3). The curves correspond to the Niatel model, eq. (2) using the fitting parameteres of Table 3. The error bars correspond to statistical uncertainties of 1 σ. The data point for the polarization voltage 400 V was not considered in the fit for the Advanced Markus chamber SN 870 and SN 879.

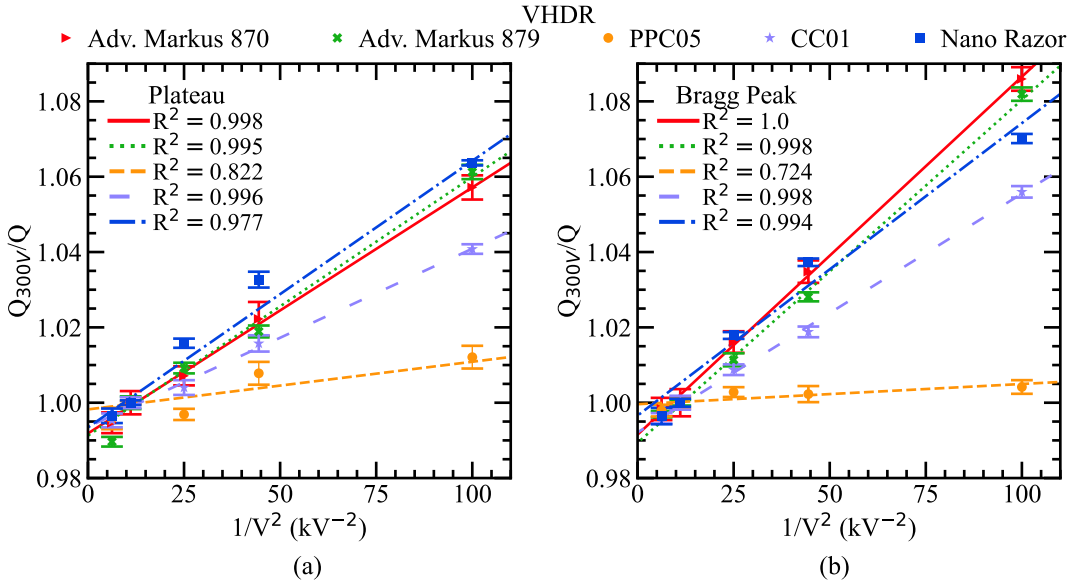

Fig. 3. The inverse of the collected charge, $1/Q$, normalized to the collected charge with the ionization chamber biased to 300 V, Q_{300V}, as a function of the inverse of the chamber's polarizing voltage, $1/V^2$, for the Advanced Markus SN 870 and SN 879, the PPC05, the CC01 and the Nano Razor CC003 chamber. The measurements in (a) were performed at the plateau of the Bragg peak, while in (b) the measurements at the Bragg peak are shown, both in VHDR conditions. The lines correspond to linear fits, respective R^2 are shown. The error bars correspond to statistical uncertainties of 1 σ. The data point for the polarization voltage 400 V was not considered in the fit for the Advanced Markus chamber SN 870 and SN 879.

Razor chamber. For the Nano Razor chamber, these results seem to suggest that initial recombination has the largest effect on the charge collection efficiency while volume recombination is negligible even at the Bragg peak, which is possibly explained by the chamber's very small volume and electrode spacing. While the increase in initial recombination from the plateau region to the Bragg peak is consistent with the increase of LET at the Bragg peak, which in turn increases same track recombination, this does not explain the observed drop in collection efficiency in VHDR irradiations. Further investigations are warranted in order to verify if other Nano Razor chambers also exhibit this behaviour at high dose rates. Moreover, it would be interesting to test in other irradiation conditions such as with different spot distributions and dose rates, as well as the dependence on the position of the chamber's stem in relation to the beam axis. Fig. 7 shows the volume recombination coefficient of the Advanced Markus chamber, measured at the entrance plateau of the Bragg peak, as a function of the instantaneous dose rate and Boag's model [27] for the respective dose rates, demonstrating that the collection efficiency can deviate significantly from this model at the highest dose rates. This model works on the assumption that, upon irradiation, the density of the generated positive ions is uniform across

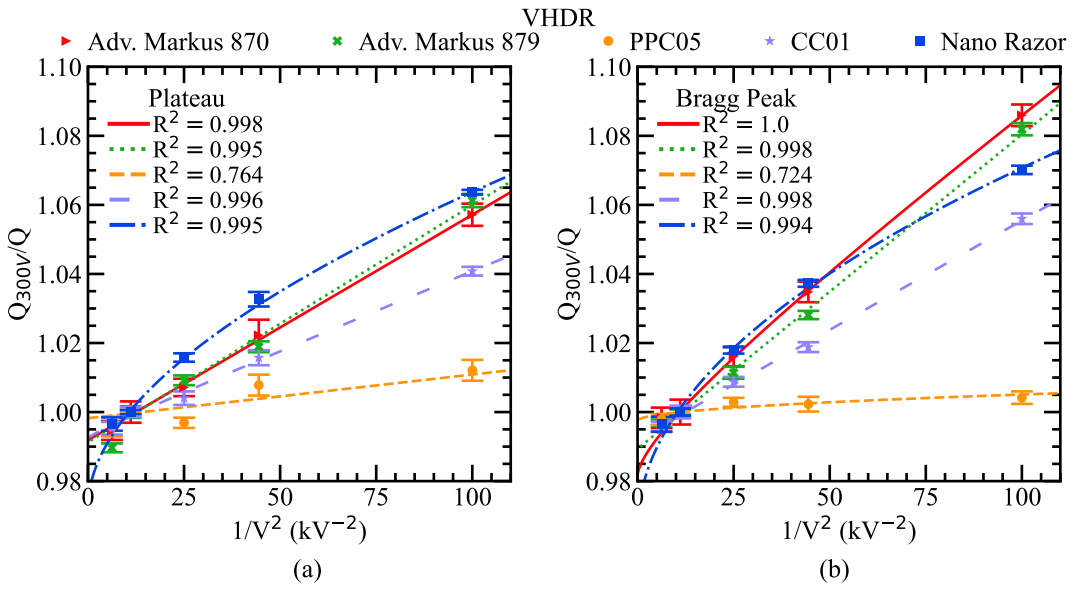

Fig. 4. The same data points as in Fig. 3 but fitted with the Niatel model as in eq. (3).

Table 3
Fitting parameters of Niatel's model, eq. (3), along with 95 % confidence intervals evaluated with the Student's *t*-distribution, for five ionization chambers in CONV (4.1 Gy/s) and VHDR (177 Gy/s and 385 Gy/s) irradiation modalities.

Ionization chamber	Mean dose rate (Gy/s)	Q_{sat}	α	β
Adv. Markus SN870	4	2.9 ± 0.1	0 ± 4	0 ± 257
	177	12 ± 1	0 ± 4	57 ± 259
	385	26 ± 3	0 ± 1	29 ± 91
Adv. Markus SN879	4.1	26.5 ± 0.8	0.1 ± 0.4	0 ± 28
	177	11.9 ± 0.7	0 ± 2	57 ± 122
	385	26 ± 1	0.0 ± 0.7	35 ± 57
PPC05	4	7.63 ± 0.05	0.1 ± 0.4	7 ± 28
	177	27.7 ± 0.6	0.0 ± 0.3	4 ± 27
	385	44.8 ± 0.6	0.0 ± 0.1	0 ± 8
Nano Razor	4	3.94 ± 0.05	0.5 ± 1	4 ± 79
	177	3.84 ± 0.06	2 ± 2	22 ± 122
	385	8.6 ± 0.1	1.3 ± 0.5	0 ± 34
CC01	4	11.95 ± 0.09	0.1 ± 0.2	2 ± 15
	177	5.18 ± 0.09	0 ± 1	85 ± 98
	385	11.14 ± 0.07	0.0 ± 0.2	57 ± 16

Table 4
Recombination coefficients, k_s for the bias voltage of 300 V, calculated with Niatel's model, the TVM and with Boag's analytical formula, for five ionization chambers in CONV (4.1 Gy/s) and VHDR (177 Gy/s and 385 Gy/s) irradiation modalities. Percentage differences between the Niatel model and TVM or Boag are shown in parenthesis.

Ionization chamber	Mean dose rate (Gy/s)	Niatel	TVM	Boag
Adv. Markus SN870	4	1.002	1.000 (−0.2 %)	1.000 (−0.2 %)
	177	1.007	1.007 (0 %)	1.007 (0 %)
	385	1.019	1.011 (−0.8 %)	1.016 (−0.3 %)
Adv. Markus SN879	4	1.008	1.002 (−0.6 %)	–
	177	1.008	1.008 (0 %)	–
	385	1.010	1.010 (0 %)	–
PPC05	4	1.002	1.001 (−0.1 %)	1.000 (−0.2 %)
	177	1.001	1.001 (0 %)	1.002 (+0.1 %)
	385	1.003	1.001 (−0.2 %)	1.003 (0 %)
Nano Razor	4	1.007	1.002 (−0.5 %)	1.000 (−0.7 %)
	177	1.030	1.008 (−2.2 %)	1.000 (−2.9 %)
	385	1.036	1.009 (−2.6 %)	1.000 (−3.5 %)
CC01	4	1.003	1.001 (−0.2 %)	–
	177	1.006	1.005 (−0.1 %)	–
	385	1.007	1.007 (0 %)	–

the chamber, which is not the case for single pencil beams. For that reason, Han et al.[45] have proposed a modification to Boag's theory in which they model the transverse ionised charge spatial distribution in the chamber with a Gaussian distribution to calculate the integral collection efficiency.

The PTW microDiamond detector measured a charge of 5.24 nC in CONV (mean dose rate of 4.1 Gy/s) and 5.02 nC in VHDR conditions (mean dose rate of 177 Gy/s) which translates to a 4 % reduction in charge collection efficiency. It is possible that this is a consequence of the dependence with the series resistance and the sensitivity of the commercially available microDiamonds, as it has been shown recently for UHDR electron beams [46]. The Razor diode, on the other hand, presented an even larger reduction; it measured a charge of 17.58 nC in CONV and 10.68 nC in the VHDR regime, which corresponds to a 39 % drop in collected charge.

4. Discussion

Commercially available ionization chambers used in proton VHDR dosimetry need to be corrected for the drop in charge collection efficiency with the dose rate due to ion recombination. Recombination coefficients were evaluated at the entrance of the plateau and at the Bragg peak of a 226.899 MeV proton beam using the Niatel model, the TVM, and Boag's analytical formula for continuous beams. A general good agreement was obtained between the three techniques with a maximum percentage difference of 2.6 % between Niatel's model and TVM. Fig. 3a and 3b show that the inverse of the chamber response as a function of the inverse square voltage is linear with a linearity coefficient, R^2, higher than 0.9 for all examined detectors except the PPC05, giving us confidence that TVM can be applied. However, in Fig. 4 the curves of the PPC05 chamber appear quite flat with the parameter α equal to 0 for the plateau region and the Bragg peak, and β much smaller than for the other chambers. This may indicate that the chamber is operating in the saturation region. It is worth noting that the PPC05 chamber, with its very small electrode gap, seems especially suited for measurements in VHDRs with recombination coefficients smaller than 0.3 %, an observation also made by Rossomme et al. [47], while the CC01 chamber also presented small recombination coefficients even for

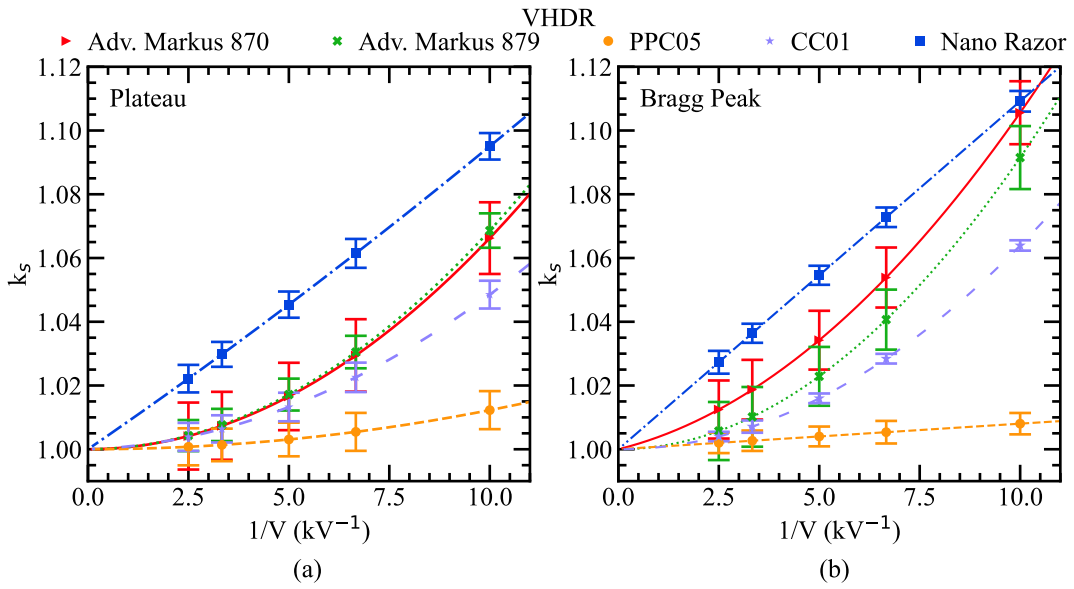

Fig. 5. k_s values as a function of the inverse of the ionization chambers's bias, $1/V$, obtained with the polynomial fit, eq. (3), at the plateau (a) and at the Bragg peak (b). The curves correspond to the Niatel model, eq. (2), using the fitting parameters. The error bars correspond to statistical uncertainties of 1σ.

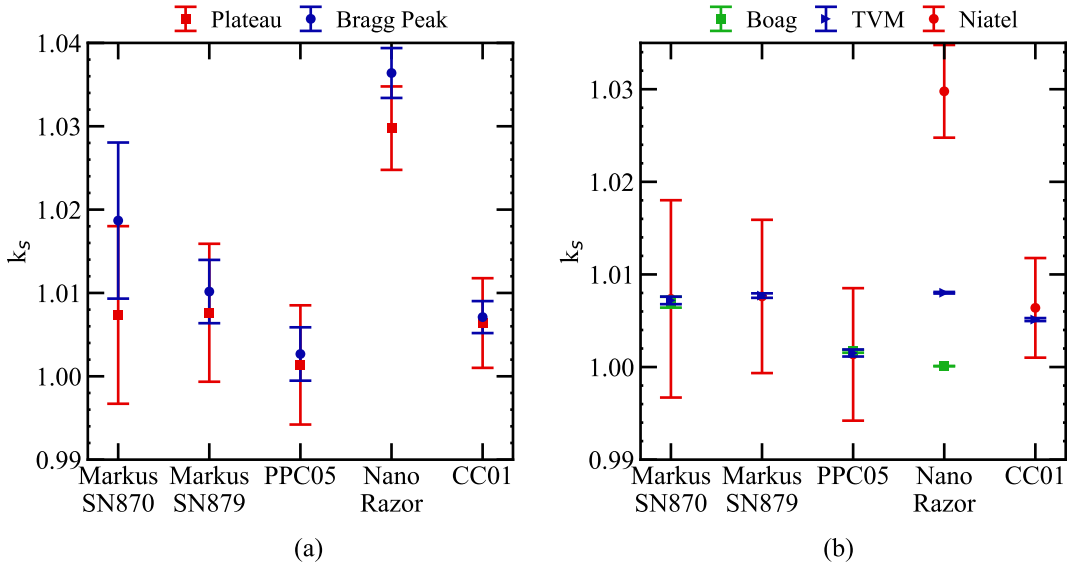

Fig. 6. (a) Recombination coefficients calculated using the Niatel model. Measurements at the plateau, corresponding to a dose rate of 177 Gy/s, and at the Bragg peak corresponding to 385 Gy/s, are shown for all the probed chambers. (b) k_s values obtained with Boag's model, the TVM and the Niatel model at the plateau region of the Bragg peak. The error bars correspond to statistical uncertainties of 1 σ.

the highest dose rates. Surprisingly, we found that the Nano Razor chamber had the highest recombination coefficient (3.6 %) among the probed chambers, even though the sensitive volume is the smallest. However, it is worth mentioning that the very small volume of the chamber might result in a higher susceptibility to dose inhomogeneities and pencil beam positioning, which can adversely increase the uncertainty in the comparison between VHDR and CONV irradiations.

For conventional irradiations our results agree with Yin et al. [34] who found k_s to be 1.003 for a mean dose rate of 1.45 Gy/s and 1.006 for 127.58 Gy/s in a DS beam line with the same energy, while we found 1.002–1.008 for 4.1 Gy/s (CONV) and 1.007–1.008 for 177 Gy/s (VHDR) for the Advanced Markus chamber. Similarly, Cunningham et al. [12] measured recombination coefficients smaller than 1.0 % in a FLASH PBS beam with mean dose rates up to 115 Gy/s. It should also be noted that the chamber's data sheet indicates that for a continuous beam the collection efficiency is ≥ 99.5 % at 187 Gy/s and ≥ 99.0 % at 375 Gy/s, regardless of beam quality. Furthermore, in VHDR conditions our results agree with Yin et al. [34] who found recombination coefficients below 1 % from unity for a variety of parallel plate chambers in a 230 MeV double-scattered proton beam with a maximum mean dose rate of 127.6 Gy/s. The results obtained in this work, therefore, confirm that standard dosimetric equipment can be used in pre-clinical FLASH experiments and clinical trials with adequate accuracy, since most probed chambers in this study have recombination coefficients smaller than 1 %.

5. Conclusion

Accurate and reliable dosimetry is a prerequisite for the implementation and understanding of preclinical FLASH-RT radiobiological experiments and mechanisms. For that reason, it is crucial to accurately assess and report the absorbed dose, the dose rate and the time structure

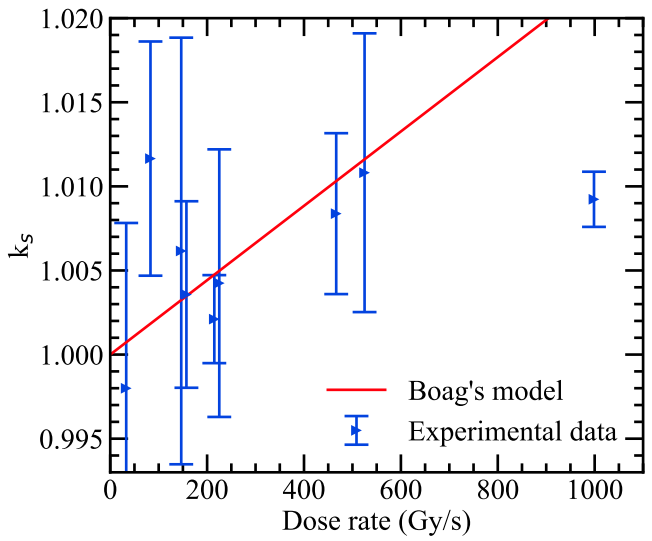

Fig. 7. The ion recombination coefficient as a function of the instantaneous dose rate for the Advanced Markus chamber and Boag's recombination model, corresponding to equation (5).

of the irradiation beams. In this study, we evaluated correction factors to be applied due to the reduction of the ion collection efficiency, for both proton CONV and VHDR conditions, for various vented ionization chambers commonly used in radiotherapy. With the exception of the Nano Razor chamber, we find that the probed chambers are suitable for absorbed dose measurements in proton VHDR scanned beams with mean dose rates up to 385 Gy/s, provided that ion recombination coefficients are taken into account.

Declaration of Competing Interest

The authors declare that they have no known competing financial interests or personal relationships that could have appeared to influence the work reported in this paper.

Acknowledgements

The authors acknowledge IBA for the support in using the machine in FLASH mode. This work was partly funded by the European Union's Horizon 2020 research and innovation program under grant agreement No. 730983 (INSPIRE). This work was partly done in the framework of the project 18HLT04 UHDpulse, which has received funding from the EMPIR program, co-financed by the Participating States and from the European Union's Horizon 2020 research and innovation program. The simulations for this work were carried out using the access to the HPC resources of TGCC under the allocation 2021-A0100312448 made by GENCI.

References

[1] Dewey DL, Boag JW. Modification of the oxygen effect when bacteria are given large pulses of radiation. Nature 1959;183:1450–1. https://doi.org/10.1038/1831450a0.
[2] Favaudon V, Caplier L, Monceau V, Pouzoulet F, Sayarath M, Fouillade C, et al. Ultrahigh dose-rate FLASH irradiation increases the differential response between normal and tumor tissue in mice. Sci Transl Med 2014;6(245). https://doi.org/10.1126/scitranslmed.3008973.
[3] Fouillade C, Curras-Alonso S, Giuranno L, Quelennec E, Heinrich S, Bonnet-Boissinot S, et al. FLASH irradiation spares lung progenitor cells and limits the incidence of radio-induced senescence. Clin Cancer Res 2020;26:1497–506. https://doi.org/10.1158/1078-0432.CCR-19-1440.
[4] Field SB, Bewley DK. Effects of dose-rate on the radiation response of rat skin. Int J Radiat Biol 1974;26:259–67. https://doi.org/10.1080/09553007414551221.
[5] Diffenderfer ES, Verginadis II, Kim MM, Shoniyozov K, Velalopoulou A, Goia D, et al. Design, implementation, and in vivo validation of a novel proton FLASH radiation therapy system. Int J Radiat Oncol Biol Phys 2020;106(2):440–8.
[6] Montay-Gruel P, Petersson K, Jaccard M, Boivin G, Germond J-F, Petit B, et al. Irradiation in a flash: Unique sparing of memory in mice after whole brain irradiation with dose rates above 100 Gy/s. Radiother Onco 2017;124:365–9. https://doi.org/10.1016/J.RADONC.2017.05.003.
[7] Montay-Gruel P, Acharya MM, Petersson K, Alikhani L, Yakkala C, Allen BD, et al. Long-term neurocognitive benefits of FLASH radiotherapy driven by reduced reactive oxygen species. Proc Natl Acad Sci USA 2019;116(22):10943–51.
[8] Simmons DA, Lartey FM, Schüler E, Rafat M, King G, Kim A, et al. Reduced cognitive deficits after FLASH irradiation of whole mouse brain are associated with less hippocampal dendritic spine loss and neuroinflammation. Radiother Onco 2019;139:4–10.
[9] Montay-Gruel P, Acharya MM, Jorge PG, Petit B, Petridis IG, Fuchs P, et al. Hypofractionated FLASH-RT as an Effective Treatment against Glioblastoma that Reduces Neurocognitive Side Effects in Mice. Clin Cancer Res 2021;27:775–84. https://doi.org/10.1158/1078-0432.CCR-20-0894.
[10] Montay-Gruel P, Bouchet A, Jaccard M, Patin D, Serduc R, Aim W, et al. X-rays can trigger the FLASH effect: Ultra-high dose-rate synchrotron light source prevents normal brain injury after whole brain irradiation in mice. Radiother Onco 2018;129(3):582–8.
[11] Hendry JH, Moore JV, Hodgson BW, Keene JP. The constant low oxygen concentration in all the target cells for mouse tail radionecrosis. Radiat Res 1982;92(1):172.
[12] Cunningham S, McCauley S, Vairamani K, Speth J, Girdhani S, Abel E, et al. Flash proton pencil beam scanning irradiation minimizes radiation-induced leg contracture and skin toxicity in mice. Cancers (Basel) 2021;13(5):1012.
[13] Bourhis J, Sozzi WJ, Jorge PG, Gaide O, Bailat C, Duclos F, et al. Treatment of a first patient with FLASH-radiotherapy. Radiother Onco 2019;139:18–22.
[14] Feasibility Study of FLASH Radiotherapy for the Treatment of Symptomatic Bone Metastases ClinicalTrials. https://clinicaltrials.gov/ct2/show/NCT04592887.
[15] Patriarca A, Fouillade C, Auger M, Martin F, Pouzoulet F, Nauraye C, et al. Experimental set-up for FLASH proton irradiation of small animals using a clinical system. Int J Radiat Oncol Biol Phys 2018;102(3):619–26.
[16] Beyreuther E, Brand M, Hans S, Hideghéty K, Karsch L, Leßmann E, et al. Feasibility of proton FLASH effect tested by zebrafish embryo irradiation. Radiother Onco 2019;139:46–50.
[17] Darafsheh A, Hao Y, Zwart T, Wagner M, Catanzano D, Williamson JF, et al. Feasibility of proton FLASH irradiation using a synchrocyclotron for preclinical studies. Med Phys 2020;47(9):4348–55.
[18] Darafsheh A, Hao Y, Zhao X, Zwart T, Wagner M, Evans T, et al. Spread-out Bragg peak proton FLASH irradiation using a clinical synchrocyclotron: Proof of concept and ion chamber characterization. Med Phys 2021;48(8):4472–84.
[19] Schüller A, Heinrich S, Fouillade C, Subiel A, De Marzi L, Romano F, et al. The European Joint Research Project UHDpulse – metrology for advanced radiotherapy using particle beams with ultra-high pulse dose rates. Phys Med 2020;80:134–50.
[20] Jolly S, Owen H, Schippers M, Welsch C. Technical challenges for FLASH proton therapy. Phys Med 2020;78:71–82. https://doi.org/10.1016/J.EJMP.2020.08.005.
[21] International Atomic Energy Agency. Absorbed Dose Determination in External Beam Radiotherapy. 2001.
[22] Almond PR, Biggs PJ, Coursey BM, Hanson WF, Huq MS, Nath R, et al. AAPM's TG-51 protocol for clinical reference dosimetry of high-energy photon and electron beams. Med Phys 1999;26(9):1847–70.
[23] Kaiser F-J, Bassler N, Tölli H, Jäkel O. Initial recombination in the track of heavy charged particles: Numerical solution for air filled ionization chambers. Acta Oncol 2012;51:368–75. https://doi.org/10.3109/0284186X.2011.626452.
[24] Boutillon M. Volume recombination parameter in ionization chambers. Phys Med Biol 1998;43(8):2061–72.
[25] Laitano RF, Guerra AS, Pimpinella M, Caporali C, Petrucci A. Charge collection efficiency in ionization chambers exposed to electron beams with high dose per pulse. Phys Med Biol 2006;51:6419–36. https://doi.org/10.1088/0031-9155/51/24/009.
[26] di Martino F, Giannelli M, Traino AC, Lazzeri M. Ion recombination correction for very high dose-per-pulse high-energy electron beams. Med Phys 2005;32:2204–10. https://doi.org/10.1118/1.1940167.
[27] Boag JW, Hochhäuser E, Balk OA. The effect of free-electron collection on the recombination correction to ionization measurements of pulsed radiation. Phys Med Biol 1996;41(5):885–97.
[28] McManus M, Romano F, Lee ND, Farabolini W, Gilardi A, Royle G, et al. The challenge of ionisation chamber dosimetry in ultra-short pulsed high dose-rate Very High Energy Electron beams. Sci Rep 2020;10(1). https://doi.org/10.1038/s41598-020-65819-y.
[29] Boag JW, Currant J. Current collection and ionic recombination in small cylindrical ionization chambers exposed to pulsed radiation. Br J Radiol 1980;53:471–8. https://doi.org/10.1259/0007-1285-53-629-471.
[30] Petersson K, Jaccard M, Germond J-F, Buchillier T, Bochud F, Bourhis J, et al. High dose-per-pulse electron beam dosimetry -A model to correct for the ion recombination in the advanced markus ionization chamber. Med Phys 2017;44(3):1157–67.
[31] Gotz M, Karsch L, Pawelke J. A new model for volume recombination in plane-parallel chambers in pulsed fields of high dose-per-pulse. Phys Med Biol 2017;62:8634–54. https://doi.org/10.1088/1361-6560/aa8985.
[32] Liszka M, Stolarczyk L, Kłodowska M, Kozera A, Krzempek D, Mojżeszek N, et al. Ion recombination and polarity correction factors for a plane-parallel ionization chamber in a proton scanning beam. Med Phys 2018;45(1):391–401.
[33] Rossomme S, Delor A, Lorentini S, Vidal M, Brons S, Jkel O, et al. Three-voltage linear method to determine ion recombination in proton and light-ion beams. Phys Med Biol 2020;65:045015. https://doi.org/10.1088/1361-6560/ab3779.

[34] Yin L, Zou W, Kim MM, Avery SM, Wiersma RD, Teo B-K, et al. Evaluation of two-voltage and three-voltage linear methods for deriving ion recombination correction factors in proton FLASH irradiation. IEEE Trans Radiat Plasma Med Sci 2022;6(3):263–70.
[35] Niatel MT. An experimental study of ion recombination in parallel-plate free-air ionization chambes. Phys Med Biol 1967;12:555. https://doi.org/10.1088/0031-9155/12/4/009.
[36] Christensen JB, Almhagen E, Stolarczyk L, Liszka M, Hernandez GG, Bassler N, et al. Mapping initial and general recombination in scanning proton pencil beams. Phys Med Biol 2020;65(11):115003.
[37] Gomà C, Lorentini S, Meer D, Safai S. Proton beam monitor chamber calibration. Phys Med Biol 2014;59:4961–71. https://doi.org/10.1088/0031-9155/59/17/4961.
[38] Karger CP, Hartmann GH. Correction of ionic recombination for pulsed radiation according to DIN 6800–2 and TRS-398. Z Med Phys 2004;14:260–6. https://doi.org/10.1078/0939-3889-00224.
[39] Palmans H, Thomas R, Kacperek A. Ion recombination correction in the Clatterbridge Centre of Oncology clinical proton beam. Phys Med Biol 2006;51(4):903–17.
[40] Boutillon M. Volume recombination parameter in ionization chambers. Phys Med Biol 1998;43:2061–72. https://doi.org/10.1088/0031-9155/43/8/005.
[41] Vilches-Freixas G, Unipan M, Rinaldi I, Martens J, Roijen E, Almeida IP, et al. Beam commissioning of the first compact proton therapy system with spot scanning and dynamic field collimation. Br J Radiol 2020:93. https://doi.org/10.1259/BJR.20190598/FORMAT/EPUB.
[42] Cavallone M, Gonçalves Jorge P, Moeckli R, Bailat C, Flacco A, Prezado Y, et al. Determination of the ion collection efficiency of the Razor Nano Chamber for ultra-high dose-rate electron beams. Med Phys 2022;49(7):4731–42.
[43] Toscano S, Souris K, Gomà C, Barragán-Montero A, Puydupin S, Stappen F vander, et al. Impact of machine log-files uncertainties on the quality assurance of proton pencil beam scanning treatment delivery. Phys Med Biol 2019;64:095021. https://doi.org/10.1088/1361-6560/AB120C.
[44] Gomà C, Sterpin E. Monte Carlo calculation of beam quality correction factors in proton beams using PENH. Phys Med Biol 2019;64:185009. https://doi.org/10.1088/1361-6560/AB3B94.
[45] Han RC, Li YJ, Pu YH. Collection efficiency of a monitor parallel plate ionization chamber for pencil beam scanning proton therapy. Nucl Sci Tech 2020;31:1–10. https://doi.org/10.1007/s41365-020-0722-z.
[46] Kranzer R, Schüller A, Bourgouin A, Hackel T, Poppinga D, Lapp M, et al. Response of diamond detectors in ultra-high dose-per-pulse electron beams for dosimetry at FLASH radiotherapy. Phys Med Biol 2022;67(7):075002.
[47] Rossomme S, Lorentini S, Vynckier S, Delor A, Vidal M, Lourenço A, et al. Correction of the measured current of a small-gap plane-parallel ionization chamber in proton beams in the presence of charge multiplication. Z Med Phys 2021;31(2):192–202.